

Geophysical Research Letters

RESEARCH LETTER

10.1029/2020GL089451

Key Points:

- The cusp region in the dayside auroral oval has been found to be the source region of dayside LSTIDs
- Enhanced energy input to the cusp initiated by IMF southward turning triggers the dayside LSTIDs
- Midlatitude LSTIDs are thermospheric gravity waves; polar cap TEC perturbations are weak polar cap patches

Supporting Information:

- Supporting Information S1
- Movie S1

Correspondence to:

Y. Nishimura,
toshi16@bu.edu

Citation:

Nishimura, Y., Zhang, S. R., Lyons, L. R., Deng, Y., Coster, A. J., Moen, J. I., et al. (2020). Source region and propagation of dayside large-scale traveling ionospheric disturbances. *Geophysical Research Letters*, 47, e2020GL089451. <https://doi.org/10.1029/2020GL089451>

Received 21 JUN 2020

Accepted 13 SEP 2020

Accepted article online 21 SEP 2020

Source Region and Propagation of Dayside Large-Scale Traveling Ionospheric Disturbances

Y. Nishimura¹ , S. R. Zhang² , L. R. Lyons³ , Y. Deng⁴ , A. J. Coster² , J. I. Moen^{5,6} ,
L. B. Clausen⁵ , W. A. Bristow⁷ , and N. Nishitani⁸ 

¹Department of Electrical and Computer Engineering and Center for Space Physics, Boston University, Boston, MA, USA,

²MIT Haystack Observatory, Westford, MA, USA, ³Department of Atmospheric and Oceanic Sciences, University of California, Los Angeles, CA, USA, ⁴Department of Physics, University of Texas at Arlington, Arlington, TX, USA,

⁵Department of Physics, University of Oslo, Oslo, Norway, ⁶Arctic Geophysics, University Centre in Svalbard, Longyearbyen, Norway, ⁷Geophysical Institute, University of Alaska Fairbanks, Fairbanks, AK, USA, ⁸Institute for Space Earth Environmental Research, Nagoya University, Nagoya, Japan

Abstract We examined the source region of dayside large-scale traveling ionospheric disturbances (LSTIDs) and their relation to cusp energy input. Aurora and total electron content (TEC) observations show that LSTIDs propagate equatorward away from the cusp and demonstrate the cusp region as the source region. Enhanced energy input to the cusp initiated by interplanetary magnetic field (IMF) southward turning triggers the LSTIDs, and each LSTID oscillation is correlated with a TEC enhancement in the dayside oval with tens of minutes periodicity. Equatorward-propagating LSTIDs are likely gravity waves caused by repetitive heating in the cusp. The cusp source can explain the high LSTID occurrence on the dayside during geomagnetically active times. Poleward-propagating Δ TEC patterns in the polar cap propagate nearly at the convection speed. While they have similar Δ TEC signatures to gravity wave-driven LSTIDs, they are suggested to be weak polar cap patches quasiperiodically drifting from the cusp into the polar cap via dayside reconnection.

1. Introduction

Large-scale traveling ionospheric disturbances (LSTIDs) are ionospheric density oscillations with \sim 1,000–3,000 km wavelength, \sim 500 m/s speed, and \sim 1–2 hr period that are coupled to gravity waves in the thermosphere (Ding et al., 2008; Tsugawa et al., 2004). LSTIDs are more frequent on the dayside, and the occurrence rate increases with geomagnetic activity (Ding et al., 2008; Tsugawa et al., 2004). LSTIDs are correlated with auroral activity, and thus, auroral processes are considered to generate LSTIDs (Chimonas & Hines, 1970; Ding et al., 2012; Hunsucker, 1982). Enhanced thermospheric heating and wind launch waves propagating away from the auroral oval as gravity waves, and ion drag creates the ionosphere density perturbation (Deng et al., 2019; Hayashi et al., 2010; Lei et al., 2008; Shiokawa et al., 2002). Thus, LSTIDs are an important manifestation of ionosphere-thermosphere coupling and energy transfer across latitudes over thousands of kilometers.

Despite that the auroral oval is likely to be the source region of LSTIDs, few studies have accurately located the source region of LSTIDs and identified the type of corresponding auroral activity. Temporal correlations between auroral electrojet and equatorward propagation of LSTIDs in the low- and middle-latitude ionosphere have often been used to infer the auroral source without locating where the actual source region is and what type of auroral processes is the driver of LSTIDs. Recent observations by Lyons et al. (2019) have addressed these questions for nightside LSTIDs. They located substorm aurora in the nightside oval and showed that nightside LSTIDs emanate from the substorm auroral region. Sheng et al. (2020) quantitatively reproduced LSTIDs in one of the events of Lyons et al. (2019).

While it is reasonable to expect that nightside auroral activity is the source of nightside LSTIDs, it does not explain the fact that dayside LSTIDs occur more often than nightside LSTIDs (Ding et al., 2008; Tsugawa et al., 2004). LSTIDs are suggested to also exist in the polar cap, and polar cap LSTIDs propagate from the dayside to nightside (Zhang et al., 2019), indicating that another source region of LSTIDs exists on the dayside. However, it is difficult to locate the dayside auroral oval solely with TEC, and radar spatial coverage is

limited compared to LSTID wavelengths. Moreover, propagating Δ TEC patterns in the polar cap should be compared to plasma flow velocity to examine whether they are LSTIDs or not.

We aim at determining the source region of dayside LSTIDs by utilizing an all-sky imager at Ny-Alesund in Svalbard (NYA, magnetic local time [MLT] = UT + 3 hr) (Moen et al., 2012) near the winter solstice on 31 December 2018, when cusp aurora was measured optically and TEC in the European and Arctic sectors detected dayside LSTIDs. We examine whether dayside LSTIDs originate in the dayside auroral oval or propagate from other regions. If the dayside auroral oval is found to be the source region of the LSTIDs, the type of aurora and possible energy of electron precipitation is determined. Properties of propagating Δ TEC patterns in the polar cap are also examined using DMSP and SuperDARN.

2. Results

2.1. Source Location

The MMS satellites were located just upstream of the bow shock ($X_{GSM} = 20 R_E$, $Y_{GSM} = 8 R_E$) and provided accurate interplanetary magnetic field (IMF) reaching the Earth during this event with a minimal (a few minutes) propagation time (Figure 1a). The IMF turned southward around 8 UT, and then the keogram from the NYA imager at 630.0 nm wavelength (*F* region emission due to low-energy electron precipitation) shows that the imager detected repetitive auroral brightenings with poleward propagation (Figure 1b). The imager was located near noon, and its location and 2-D structure of the dayside aurora can be found in Figure 2. Figures 2b and 2g show two of the brightenings, which are discrete auroral intensifications near noon. The repetitive poleward-propagating auroral brightenings are called poleward moving auroral forms (PMAFs), which are typical cusp auroral signatures (Frey et al., 2019, and references therein). Thus, the imager covered at least a portion of the cusp aurora during this event. The poleward and equatorward boundaries of the dayside auroral oval (sharp luminosity gradients marked by the solid lines in Figure 1b) moved equatorward during the PMAFs, as is an expected response to the IMF southward turning.

Vertical TEC data at each line of sight (LOS) were calculated every 60 s using the Global Positioning System (GPS) and Global Navigation Satellite System (GLONASS) above 30° elevation, and Δ TEC data were created using the Savitzky-Golay filter with a 1-hr sliding window (similar to Zhang et al., 2019). The use of GLONASS has an advantage of increasing data coverage in the polar region, where the number of receivers is limited. The maximum magnitudes of Δ TEC and TEC every 1° magnetic latitude (MLAT) and every 60 s over Europe and Greenland (70–135° magnetic longitude (MLON), where most dayside data exist) were calculated to create the keograms of Δ TEC and TEC data in Figures 1c and 1d. The dayside auroral oval boundaries were copied from Figure 1b. The optical boundaries coincided roughly with the weakly enhanced TEC around 75° MLAT. Figure 1c shows poleward-propagating Δ TEC patterns in the auroral oval and polar cap, and equatorward-propagating Δ TEC patterns at midlatitudes. Here we focus on describing propagating Δ TEC patterns, and we discuss their relation to LSTIDs in Section 2.2. Two-dimensional structures of the propagating Δ TEC patterns that were found between 10:15 and 13:00 UT are marked in Figure 2. Movie S1 in the supporting information gives the image sequence every 1 min. Corresponding TEC maps are shown in Figure S2. Each equatorward-propagating Δ TEC front first appeared near the equatorward boundary of the dayside auroral oval after a cusp auroral brightening and mainly propagated equatorward. The poleward-propagating Δ TEC patterns rapidly propagated poleward into the polar cap. Equatorward-propagating Δ TEC propagated toward midlatitudes at a slower speed, longer wavelength, and smaller amplitude. Within the available TEC data coverage, the Δ TEC signals did not propagate from other regions but propagated away from the dayside auroral oval near noon. The Δ TEC propagation away from the dayside auroral oval strongly indicates that the source region of the dayside Δ TEC is the cusp region. The Δ TEC enhancements were activated soon after the IMF southward turning, which supports the idea that enhanced energy input from the solar wind to the dayside auroral oval creates the dayside Δ TEC enhancements and propagation.

The longitudinal coverage of aurora and TEC is not sufficiently wide to determine the longitudinal extent of the aurora and Δ TEC enhancements. Nevertheless, the enhancements of Δ TEC and aurora in the auroral oval in Figures 2b and 2g extended in total over 5–6 hr of MLT around noon. This is comparable to the typical cusp width (Zhang et al., 2013). The polar cap and midlatitude Δ TEC enhancements were seen almost over the entire MLTs that were covered in TEC ($> \sim 4$ and $> \sim 8$ hr MLT widths, respectively). Within the available

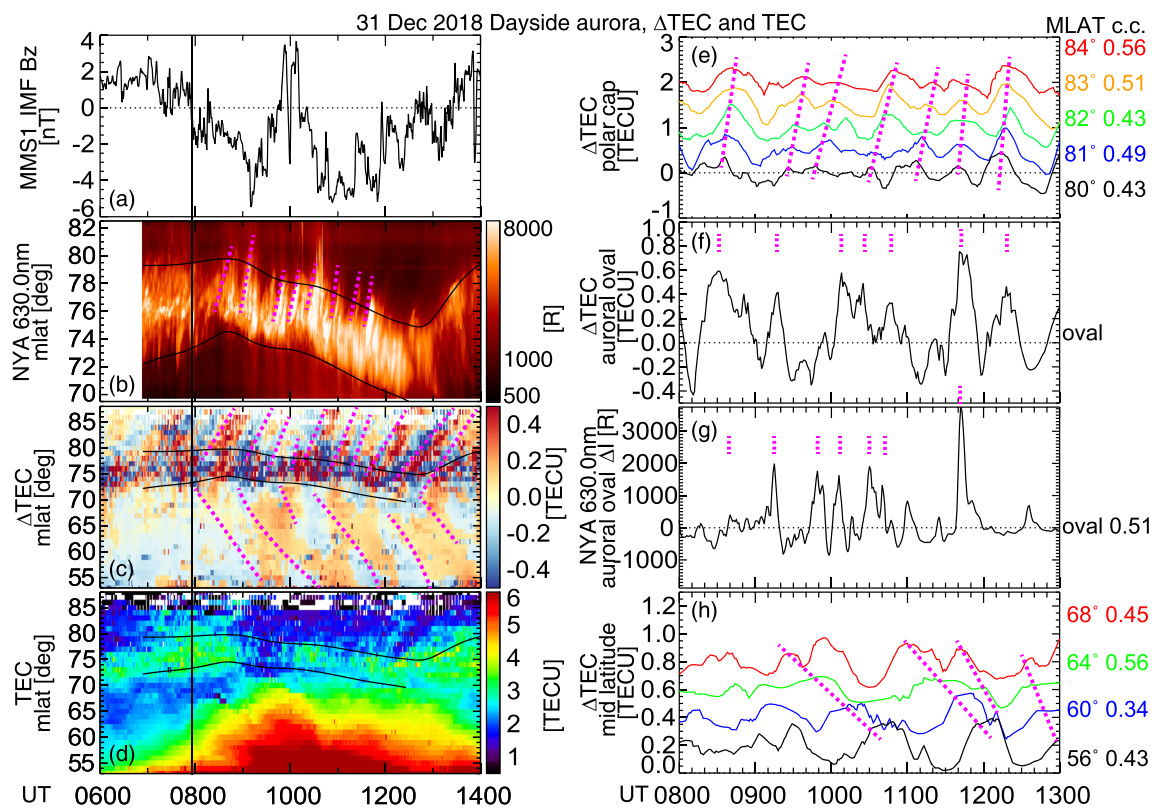


Figure 1. Left: (a) IMF B_z measured by MMS-1 and north-south keograms of (b) 630.0 nm aurora at NYA, (c) Δ TEC at 70–135° MLON (Europe and Greenland), and (d) TEC keograms on 31 December 2018. The IMF southward turning is marked by the vertical solid line. The horizontal solid lines in panels (b)–(d) mark the poleward and equatorward boundaries of the auroral oval. The pink dashed lines visually trace the PMAFs and Δ TEC enhancements. The magnetic noon at the imager location is at 9 UT. Typical 230 km emission altitude and 300 km pierce point altitude are used. Right: (e) Δ TEC from panel (c) in the polar cap at 80–84° MLAT, (f) Δ TEC averaged in the auroral oval, (g) 630.0 nm auroral intensity in the auroral oval high-pass filtered at 1 hr cutoff period, and (h) Δ TEC at midlatitudes at 68°, 64°, 60°, and 56° MLAT. Correlation coefficients between Δ TEC at each latitude and Δ TEC in the oval (panel f) are shown next to the MLAT labels. Maximum correlations within 1 hr (polar cap) and 2 hr (midlatitude) lags are presented. Δ TEC at each latitude is arbitrarily shifted vertically.

spatial coverage, the azimuthally wide dayside source could explain the wide azimuthal extent of the Δ TEC enhancements.

The line plots in Figures 1e–1h present correlations between the Δ TEC in the polar cap and midlatitudes (Figures 1e and 1h) and Δ TEC in the auroral oval (Figure 1f). Many of the Δ TEC enhancements in the auroral oval corresponded to the quasiperiodic PMAF auroral intensifications (Figure 1g, 0.51 correlation coefficient). The Δ TEC enhancements in the oval are likely due to ionization by electron precipitation. The poleward-propagating Δ TEC patterns in the polar cap (Figure 1e) have a nearly one-to-one correspondence with Δ TEC in the oval with >0.4 correlation coefficient, where time lags were considered and they were within ~ 30 min. The oscillation period is ~ 30 min. The equatorward-propagating Δ TEC patterns at midlatitudes have a longer period of ~ 50 –90 min than do the poleward-propagating Δ TEC patterns. They do not respond to individual PMAFs but appear to occur in association with the longer-lasting Δ TEC enhancements in the oval. For both polar cap and midlatitude Δ TEC signals, the oscillation periods are not constant but change over time. The variable time periods suggest that the individual Δ TEC pulses are driven by transient energy input to the dayside auroral oval. Note, however, that the correlations are not perfect. Density transport in the oval may obscure the Δ TEC signals in the oval. Also, the TEC measurement locations change over time as the Global Navigation Satellite System (GNSS) satellites fly through space, the spatial resolution of TEC in the auroral oval is not as dense as at midlatitudes, and ionospheric density and auroral emission reflect different physics. These limitations may contribute to lower the correlation.

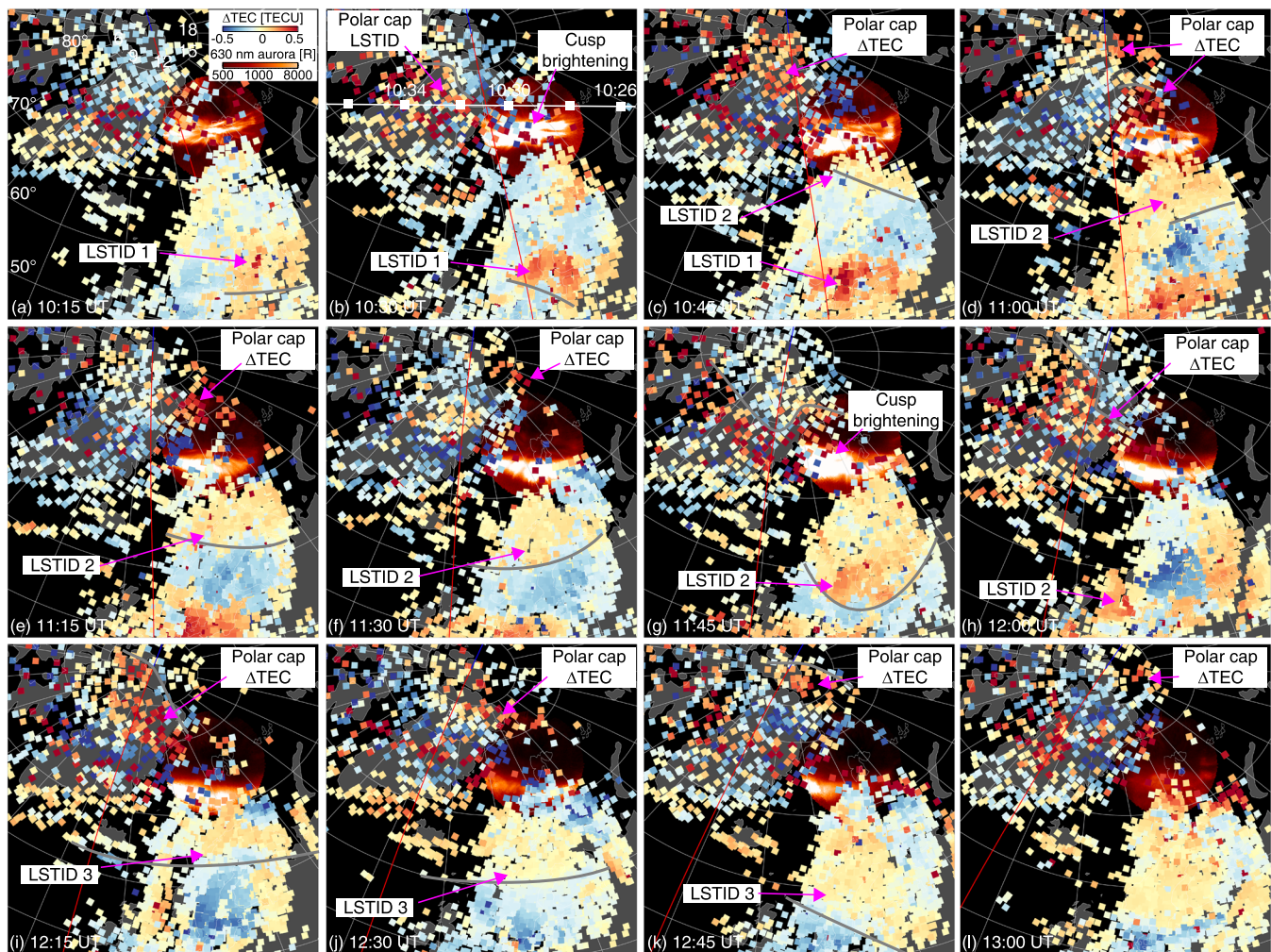


Figure 2. (a–l) Selected 2-D images of the ΔTEC and 630.0 nm aurora data projected over the map. The red line marks the magnetic noon. The white contours are latitude (every 10°) and longitude (every 15°) contours. The fronts of the poleward and equatorward ΔTEC enhancements are marked by the gray lines. Panel (b) shows the trajectory of DMSP-18. Movie S1 shows the images every 1 min.

2.2. Propagation Speed

Figure 3 estimates the meridional propagation speeds of the ΔTEC and compares them to SuperDARN and DMSP observations. Because ΔTEC in this event propagated mainly meridionally (Figure 2), the meridional velocity represents the ΔTEC propagation velocity. By calculating the slopes in ΔTEC , the poleward velocities of the polar cap were found to be 1.2 ± 0.2 (before 12 UT) and ~ 0.4 km/s (after 12 UT). The slowdown of the ΔTEC seems to coincide with the IMF northward turning (Figure 1a) and a reduction of the poleward convection speed (Figures 3d and 3e, see below for more details). The equatorward-propagating ΔTEC propagated at 0.37 ± 0.11 km/s on average. This speed is within the range of typical LSTID speed (Ding et al., 2008; Tsugawa et al., 2004), and the amplitude satisfies the >0.1 total electron content unit (TECU) threshold used by Figueiredo et al. (2017). These are likely LSTIDs and are attributed to gravity waves (Shiokawa et al., 2002).

To evaluate more properties of the poleward-propagating ΔTEC patterns, we compared this speed with plasma velocity measured by DMSP. DMSP-18 passed one of the ΔTEC enhancements at 10:31:30–10:34:00 UT as shown in Figure 2b. The auroral poleward boundary (cutoff of approximately keV electron precipitation) along the orbit was located at 75.5° MLAT at 9 MLT (Figure 3l). The enhanced density at 10:31:30–10:34:00 UT (Figure 3i) was in the polar cap, and it was more elevated than in the rest of the

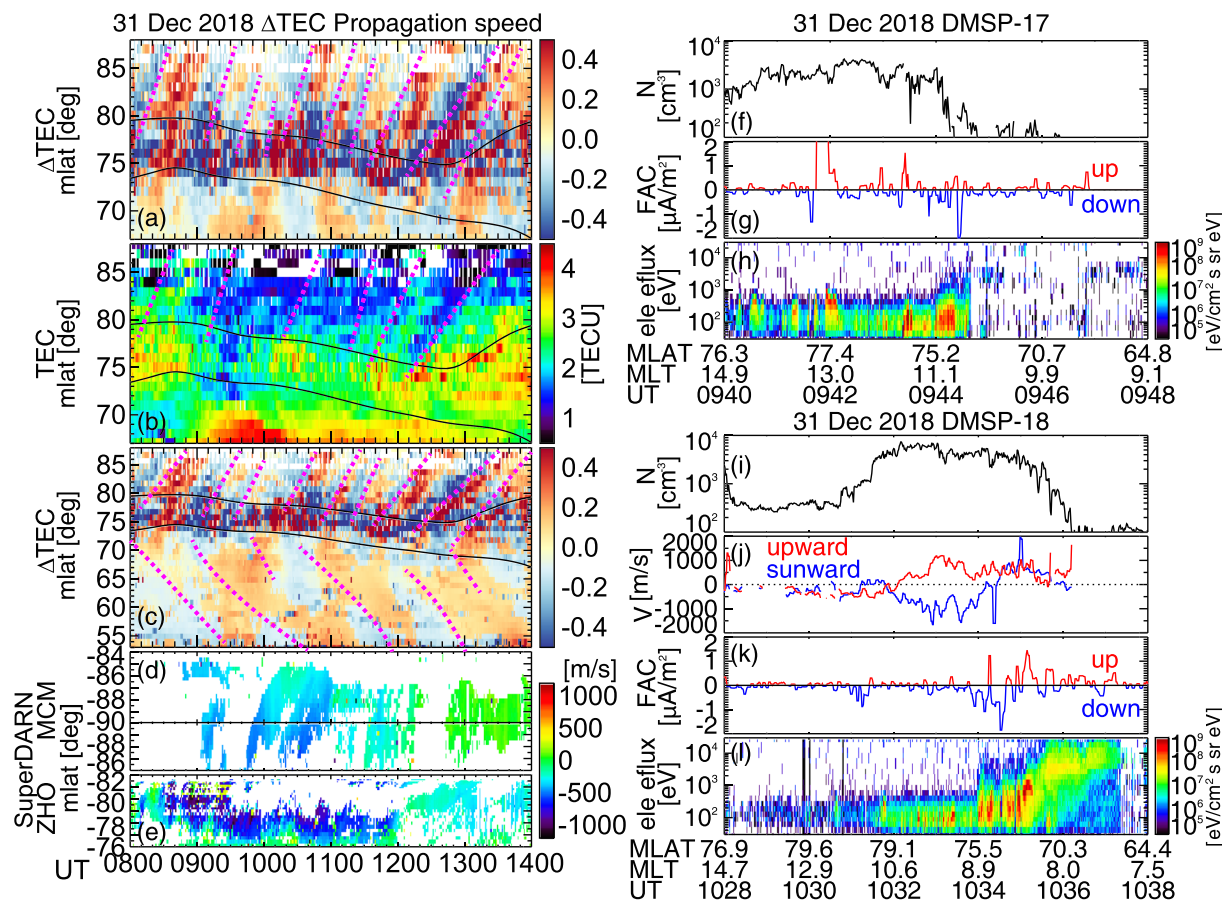


Figure 3. (a) ΔTEC and (b) TEC keograms above 67° MLAT, (c) ΔTEC keogram above 53° MLAT, and SuperDARN LOS velocity (positive sunward) at (d) MCM at Beam 9 and (e) ZHO at Beam 15. (f–h) DMSP-17 measurements of the density, FAC, and electron energy flux. (i–l) DMSP-18 measurements of the density, velocity, FAC, and electron energy flux. DMSP-17 does not provide reliable drift measurements in this event. See also SuperDARN convection maps in Figure S3.

polar cap (before 10:31:30 UT). The density ($4,630 \pm 800 \text{ cm}^{-3}$) was also about twice as high as the density measured by DMSP-17 ($2,330 \pm 720 \text{ cm}^{-3}$, Figure 3f) 50 min earlier during a period of weaker ΔTEC magnitude. The high-density plasma in the polar cap satisfies the definition of a polar cap patch (more than twice the background density; Crowley, 1996), but it is a weak patch because the density is considerably lower than well-developed patches (e.g., Nishimura et al., 2014). Some of the poleward-propagating ΔTEC can also be seen in the TEC keogram in Figure 3b, and thus, the polar cap ΔTEC are associated with a substantial increase of TEC with respect to the background.

The cross-track antisunward velocity at DMSP-18 over the region of enhanced ΔTEC was $0.84 \pm 0.21 \text{ km/s}$. The cross-track direction was 23° away from the magnetic north. If the flow was mainly poleward and DMSP measured the cross-track component of it, the maximum possible poleward flow was $0.92 \pm 0.23 \text{ km/s}$. This velocity is comparable to the propagation speed of the poleward-propagating ΔTEC . The field-aligned currents (FACs) calculated from magnetic field data in the prenoon auroral oval (10:34–10:35 UT, Figure 3k) were more enhanced than at 09:44 UT (Figure 3g). However, given that DMSP was away from the cusp, we cannot discuss how FACs in the cusp changed.

While DMSP only provided a snapshot of the polar cap flow, the SuperDARN radars in Antarctica measured plasma velocity for a longer time period (no radar data available on the dayside in the Northern Hemisphere). The McMurdo (MCM) and Zhongshan (ZHO) radars measured LOS velocity in the dayside polar region. Echo locations and convection maps can be found in Figure S3. The ZHO radar detected sustained velocity away from the radar ($0.64 \pm 0.08 \text{ km/s}$ when the radar covered near noon at 08:30–10:00 UT, Figure 3e), and the enhanced flows extended across the magnetic pole with decreasing speed as the flows progressed

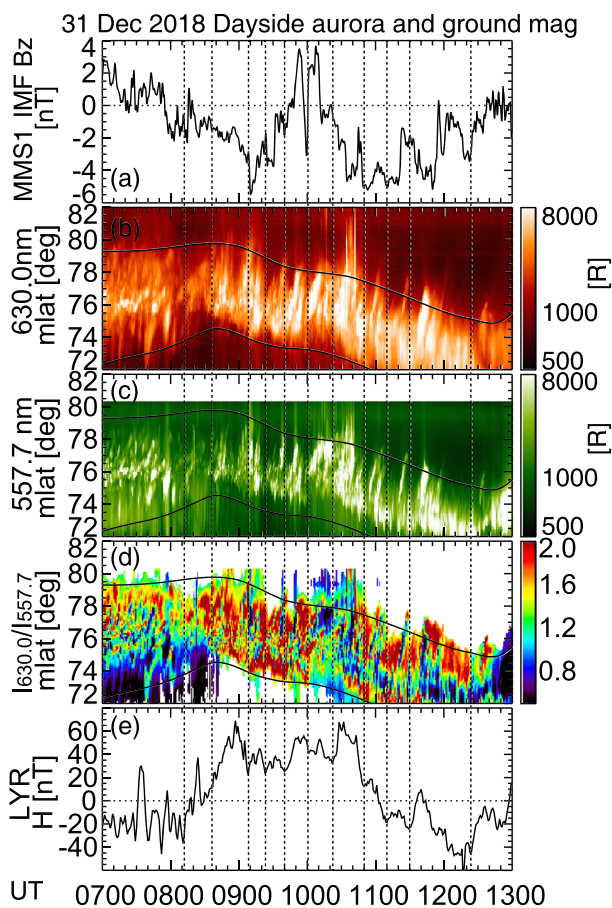


Figure 4. (a) IMF B_z by MMS1, (b) 630.0 nm, (c) 557.7 nm, and (d) intensity ratio keograms at NYA and (e) the H -component of the LYR magnetometer data. The intensity ratio is calculated where the 557.7 nm intensity is above 1 kR to avoid airglow and noise.

The intensity ratio decreased to <1 during intense PMAFs (e.g., 10:10–10:20 UT), suggesting a contribution of approximately keV electrons during those times. Each PMAF was also associated with a small enhancement of the H component of the ground magnetic field (Figure 4e). The connection between the PMAFs and ground magnetic field indicates formation of enhanced precipitation and a wedge-shaped current system during dayside reconnection (Milan et al., 2000). By also considering the enhanced poleward flows measured by SuperDARN, the enhanced plasma density in the cusp created by precipitation is transported poleward during dayside reconnection and then becomes weak polar cap patches. The dayside reconnection and related precipitation are repetitive and thus can be seen as repetitive weak patch formation.

3. Conclusion

We investigated a dayside LSTID event using TEC and auroral imaging to examine the source region of the dayside LSTIDs during a day with excellent observational coverage. We found that the cusp was the source region of the dayside LSTIDs. The LSTIDs were activated by the IMF southward turning and enhanced electron precipitation into the cusp, indicating that enhanced energy input from the solar wind to the cusp created the dayside LSTIDs. The equatorward-propagating LSTIDs first appeared just equatorward of the cusp and propagated toward midlatitudes. The LSTIDs are associated with TEC modulations with tens of minutes periodicity in the dayside auroral oval. The waves are not coherent, but the interval between the pulses is variable. This suggests that time-varying energy input to the cusp repetitively heat the thermosphere and drove the LSTIDs. The cusp has also been shown as the source of medium-scale TIDs (MSTIDs) (Bristow et al., 1994), and thus, energy input to the cusp could create a wide spectral range of disturbances.

away from the dayside oval (Figure 3d). As shown in Figure S3, the plasma flows near noon at $\sim 80^\circ$ MLAT were nearly poleward. The averaged poleward velocity at 08:30–10:00 UT was 1.06 ± 0.13 km/s, and then the velocity dropped to a few hundred m/s at 12 UT in association with the IMF northward turning and deceleration of the Δ TEC. Although these velocities measured in the Southern Hemisphere only serve as a reference for the observations in the Northern Hemisphere, the velocity magnitudes and the slowdown over time are consistent with the evolution of the poleward-propagating Δ TEC.

Both DMSP and SuperDARN observations suggest that poleward-propagating Δ TEC patterns in the polar cap propagated approximately at the poleward $E \times B$ drift speed. By also considering the association with the polar cap patch seen by DMSP, they are likely small polar cap patches that repetitively propagate from the cusp into the polar cap rather than gravity waves.

2.3. Precipitation and Current

Figure 4 shows the IMF, auroral intensities at 630.0 and 557.7 nm, the intensity ratio, and the H -component of the magnetic field in Longyearbyen (LYR, located near the imager site). The 557.7 nm aurora shows PMAFs in a similar manner as in 630.0 nm wavelength. The ratio of 630.0 and 557.7 nm is inversely proportional to the precipitating electron energy (Rees & Luckey, 1974) and thus can be used to deduce the energy of precipitating electrons during the LSTIDs. Soon after the IMF southward turning (~ 8 UT), the intensities at both wavelengths and the intensity ratio increased, indicating that the soft electron flux of a few 100 eV increased. The enhanced soft electron precipitation would increase the F region ionosphere density and become the source of the weak patches. Thermosphere heating by the soft electron precipitation and Joule heating by related fast flows (Skjæveland et al., 2017) would explain the equatorward-propagating LSTIDs.

Propagating Δ TEC patterns away from the cusp were also seen in the polar cap and show a nearly one-to-one correspondence with the repetitive cusp auroral intensifications (PMAFs). The propagation speed of the poleward-propagating Δ TEC patterns (~ 1 km/s during the southward IMF and ~ 0.4 km/s during small IMF(B_z)) is comparable to the plasma drift speed measured by DMSP and SuperDARN. The TEC change can be seen in the absolute TEC data, and DMSP detected a weak polar cap patch when it traversed one of the poleward-propagating LSTIDs pulses. We suggest that the polar cap Δ TEC patterns are not LSTIDs coupled to gravity waves but are weak polar cap patches, which are consistent with traditional understanding of patch formation as F region density structures that are created by cusp precipitation and then drift into the polar cap.

Thermosphere heating could also create LSTIDs propagating poleward, but we did not detect a clear Δ TEC propagation in the polar cap as slow as the equatorward-propagating LSTIDs. LSTIDs by gravity waves require inclined magnetic field and density gradient in order to be seen in TEC (Shiokawa et al., 2002). Even if traveling atmospheric disturbances exist in the polar cap thermosphere, corresponding TEC perturbation may be too small to be detected due to large magnetic field inclination and low background density. Zhang et al. (2019) suggested existence of polar cap LSTIDs, but their event lacks convection observation. The present event analysis indicates that they may not be LSTIDs, although it is an open question if this conclusion applies to other events or if there are events with gravity waves driving polar cap LSTIDs.

While more observation intervals need to be considered, the cusp source could provide the solution to the higher occurrence of LSTIDs on the dayside than nightside. Because the energy input to the cusp increases with geomagnetic activity, the cusp source is also consistent with the higher occurrence of LSTIDs during geomagnetically active times.

Data Availability Statement

Data were obtained through the sites (cedar.openmadrigal.org, tid.uio.no/plasma/aurora, vt.superdarn.org, and themis.ssl.berkeley.edu). Data processing used SPEDAS-V3.1 (Angelopoulos et al., 2019). GNSS data are provided by participating organizations (see Text S4 for the full list).

Acknowledgments

This work was supported by NASA NNX17AL22G, 80NSSC18K0657 and 80NSSC20K0604, NSF AGS-1907698 and AGS-1762141, and AFOSR FA9559-16-1-0364. J. I. M. and L. B. N. C. acknowledge support by Research Council of Norway Grant 275653. We thank support from the CEDAR workshop “Grand Challenge: Multi scale I-T system dynamics” and ISSI workshops “Multiple-instrument observations and simulations of the dynamical processes associated with polar cap patches/aurora and their associated scintillations” and “Multi-Scale Magnetosphere-Ionosphere-Thermosphere Interaction.”

References

Angelopoulos, V., Cruce, P., Drozdov, A., Grimes, E. W., Hatzigeorgiu, N., King, D. A., et al. (2019). *Space Science Reviews*, 215(1), 9. <https://doi.org/10.1007/s11214-018-0576-4>

Bristow, W. A., Greenwald, R. A., & Samson, J. C. (1994). Identification of high-latitude acoustic gravity wave sources using the Goose Bay HF radar. *Journal of Geophysical Research*, 99(A1), 319–331. <https://doi.org/10.1029/93JA01470>

Chimonas, G., & Hines, C. O. (1970). Atmospheric gravity waves launched by auroral currents. *Planetary and Space Science*, 18(4), 565–582. [https://doi.org/10.1016/0032-0633\(70\)90132-7](https://doi.org/10.1016/0032-0633(70)90132-7)

Crowley, G. (1996). Critical review of ionospheric patches and blobs. In W. R. Stone (Ed.), *Review of radio science* (Chap. 27, pp. 619–648). New York: Oxford University press.

Deng, Y., Heelis, R., Lyons, L. R., Nishimura, Y., & Gabrielse, C. (2019). Impact of flow bursts in the auroral zone on the ionosphere and thermosphere. *Journal of Geophysical Research: Space Physics*, 124, 10,459–10,467. <https://doi.org/10.1029/2019JA026755>

Ding, F., Wan, W., Liu, L., Afraimovich, E. L., Voeykov, S. V., & Pervelova, N. P. (2008). A statistical study of large-scale traveling ionospheric disturbances observed by GPS TEC during major magnetic storms over the years 2003–2005. *Journal of Geophysical Research*, 113, A00A01. <https://doi.org/10.1029/2008JA013037>

Ding, F., Wan, W., Ning, B., Zhao, B., Li, Q., Zhang, R., et al. (2012). Two-dimensional imaging of large-scale traveling ionospheric disturbances over China based on GPS data. *Journal of Geophysical Research*, 117, A08318. <https://doi.org/10.1029/2012JA017546>

Figueiredo, C. A. O. B., Wrassse, C. M., Takahashi, H., Otsuka, Y., Shiokawa, K., & Barros, D. (2017). Large-scale traveling ionospheric disturbances observed by GPS dTEC maps over North and South America on Saint Patrick’s Day storm in 2015. *Journal of Geophysical Research: Space Physics*, 122, 4755–4763. <https://doi.org/10.1002/2016JA023417>

Frey, H. U., Han, D., Kataoka, R., Lessard, M. R., Milan, S. E., Nishimura, Y., et al. (2019). Dayside aurora. *Space Science Reviews*, 215(8), 51. <https://doi.org/10.1007/s11214-019-0617-7>

Hayashi, H., Nishitani, N., Ogawa, T., Otsuka, Y., Tsugawa, T., Hosokawa, K., & Saito, A. (2010). Large-scale traveling ionospheric disturbance observed by superDARN Hokkaido HF radar and GPS networks on 15 December 2006. *Journal of Geophysical Research*, 115, A06309. <https://doi.org/10.1029/2009JA014297>

Hunsucker, R. D. (1982). Atmospheric gravity waves generated in the high-latitude ionosphere: A review. *Reviews of Geophysics*, 20(2), 293–315. <https://doi.org/10.1029/RG020i002p00293>

Lei, J., Burns, A. G., Tsugawa, T., Wang, W., Solomon, S. C., & Wiltberger, M. (2008). Observations and simulations of quasiperiodic ionospheric oscillations and large-scale traveling ionospheric disturbances during the December 2006 geomagnetic storm. *Journal of Geophysical Research*, 113, A06310. <https://doi.org/10.1029/2008JA013090>

Lyons, L. R., Nishimura, Y., Zhang, S.-R., Coster, A. J., Bhatt, A., Kendall, E., & Deng, Y. (2019). Identification of auroral zone activity driving large-scale traveling ionospheric disturbances. *Journal of Geophysical Research: Space Physics*, 124, 700–714. <https://doi.org/10.1029/2018JA025980>

Milan, S. E., Lester, M., Cowley, S. W. H., & Brittnacher, M. (2000). Convection and auroral response to a southward turning of the IMF: Polar UVI, CUTLASS, and IMAGE signatures of transient magnetic flux transfer at the magnetopause. *Journal of Geophysical Research*, 105(A7), 15,741–15,755. <https://doi.org/10.1029/2000JA900022>

Moen, J., Carlson, H. C., Rinne, Y., & Skjæveland, Å. (2012). Multi-scale features of solar terrestrial coupling in the cusp ionosphere. *Journal of Atmospheric and Solar - Terrestrial Physics*, 87–88, 11–19. <https://doi.org/10.1016/j.jastp.2011.07.002>

Nishimura, Y., Lyons, L. R., Zou, Y., Oksavik, K., Moen, J. I., Clausen, L. B., et al. (2014). Day-night coupling by a localized flow channel visualized by polar cap patch propagation. *Geophysical Research Letters*, 41, 3701–3709. <https://doi.org/10.1002/2014GL060301>

Rees, M. H., & Luckey, D. (1974). Auroral electron energy derived from ratio of spectroscopic emissions 1. Model computations. *Journal of Geophysical Research*, 79(34), 5181–5186. <https://doi.org/10.1029/JA079i034p05181>

Sheng, C., Deng, Y., Zhang, S.-R., Nishimura, Y., & Lyons, L. R. (2020). Relative contributions of ion convection and particle precipitation to exciting large-scale traveling atmospheric and ionospheric disturbances. *Journal of Geophysical Research: Space Physics*, 125, e2019JA027342. <https://doi.org/10.1029/2019JA027342>

Shiokawa, K., Otsuka, Y., Ogawa, T., Balan, N., Igarashi, K., Ridley, A. J., et al. (2002). A large-scale traveling ionospheric disturbance during the magnetic storm of 15 September 1999. *Journal of Geophysical Research*, 107(A6), 1088. <https://doi.org/10.1029/2001JA000245>

Skjæveland, Å. S., Carlson, H. C., & Moen, J. I. (2017). A statistical survey of heat input parameters into the cusp thermosphere. *Journal of Geophysical Research: Space Physics*, 122, 9622–9651. <https://doi.org/10.1002/2016JA023594>

Tsugawa, T., Saito, A., & Otsuka, Y. (2004). A statistical study of large-scale traveling ionospheric disturbances using the GPS network in Japan. *Journal of Geophysical Research*, 109, A06302. <https://doi.org/10.1029/2003JA010302>

Zhang, B., Brambles, O., Lotko, W., Dunlap-Shohl, W., Smith, R., Wiltberger, M., & Lyon, J. (2013). Predicting the location of polar cusp in the Lyon-Fedder-Mobarry global magnetosphere simulation. *Journal of Geophysical Research: Space Physics*, 118, 6327–6337. <https://doi.org/10.1002/jgra.50565>

Zhang, S.-R., Erickson, P. J., Coster, A. J., Rideout, W., Vierinen, J., Jonah, O., & Goncharenko, L. P. (2019). Subauroral and polar traveling ionospheric disturbances during the 7–9 September 2017 storms. *Space Weather*, 17, 1748–1764. <http://doi.org/10.1029/2019SW002325>